Analytical and numerical techniques in the Green's function treatment of microstrip antennas and scatterers

J.R. Mosig and Prof. F.E. Gardiol, M.Sc., D. Appl. Sc., S. Mem. IEEE

Indexing terms: Antennas, Microwave components, Numerical analysis, Dielectrics

Abstract: In the paper, the mode theory of wave propagation in stratified media is used to establish the spatial Green's functions associated with a microstrip structure. They correspond to the fields and potentials created by a horizontal electric dipole placed on the air/dielectric interface and are expressed as Sommerfeld integrals. Near- and far-field approximate analytical evaluations of these integrals are rigorously derived. They allow a quantitative discussion of the scope and limitations of the static microstrip theory, and point out the relevance of surface wave effects in microstrip. The most interesting situation when both source and observer are in the air/dielectric interface is studied extensively. Numerical methods to evaluate Sommerfeld integrals in such situations are reviewed, and several new accurate techniques are introduced and discussed in detail.

1 Introduction

Microstrip structures are now widely used in microwave systems, mainly in situations where a low profile, small size and mechanical ruggedness are the fundamental design specifications to be met. Typical applications include antennas for aircraft/satellite communication links [1], and cancer treatment by hyperthermia [2]. Moreover, microstrip structures are easy and inexpensive to fabricate and well adapted for industrial processing.

While simple structures such as circular or rectangular isolated patches have been analysed with relatively simple models [3], the increasing complexity of many structures, now in current use, calls for a more elaborate theoretical model. Among its principal features, the model must be able to handle arbitrary geometries and permittivities at any frequency. In addition, not only the radiation pattern but the near-field values, the coupling between adjacent structures and the launching of surface waves must be inferred from this model.

The most promising way to develop such a model is to consider the microstrip structure as a particular case of a stratified medium. The pioneer study on electromagnetic-wave propagation in stratified media must be ascribed to Sommerfeld, who investigated the radiowave propagation above a lossy ground as early as 1909. Later, several authors [4–6] have extended these theories to arbitrary stratified media, and quite recently this model has been applied to practical microstrip structures [7–8].

Two specific features arise when applying Sommerfeld's model to microstrip. First, the losses do not play a significant role and may even be neglected in some practical situations. Secondly, the fields are created by electric surface currents which lie in the air/dielectric interface and, if these currents are calculated by solution of an integral equation, the observation point must also be in the interface. These facts influence particulary the evaluation of the Green's functions for which the theory gives an integral representation. Many numerical and approximate analytical methods in stratified media take advantage of some properties of integrands related to significant losses, or to a height difference between source and observer. These methods lose a substantial part of their effectiveness or even do not work at all in microstrip problems.

Paper 2354 H, first received 26th April and in revised form 10th September 1982

The authors are with the École Polytechnique Fédérale de Lausanne, Département d'Électricité, Laboratoire d'Electromagnétisme et d'Acoustique, 16ch. de Bellerive, CH-1007 Lausanne, Switzerland

This paper reviews the theoretical foundations of a microstrip dynamical model and sets up approximate analytical and numerical methods to evaluate the fields on the interface of a microstrip structure. Particular attention is paid to the development of efficient numerical techniques. The algorithms introduced are quite general and can also be applied to similar integral expressions, such as Fourier transforms or Fourier-Bessel (Hankel) transforms, currently found in related fields of applied physics.

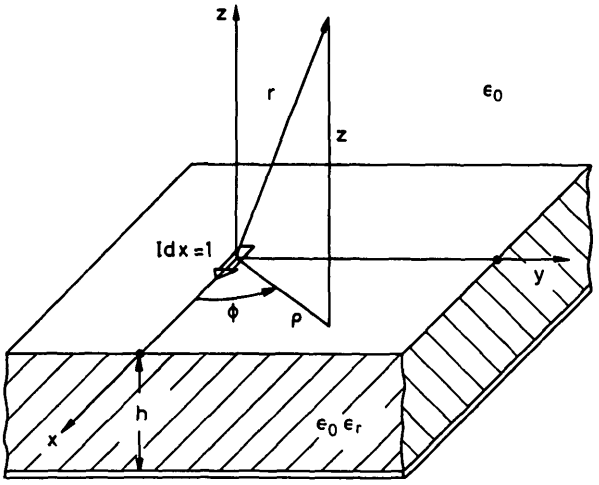

Fig. 1 *Horizontal electric dipole (HED) on a microstrip structure*

2 Horizontal electric dipole on microstrip

The first step in the study of an arbitrary microstrip structure is the determination of the fields created by a horizontal electric dipole (HED) situated along the x-axis in the air/dielectric interface (Fig. 1), and having a unit moment ($Idx = 1$).

Following Harrington [9], these fields will be derived from a scalar and a vector potential as

$$E = -j\omega A - \nabla V \tag{1}$$

$$H = \frac{1}{\mu_0} \nabla \times A \tag{2}$$

Several other approaches to determine the fields, such as decomposition into their TM and TE parts, are also currently used [6]. But the use of potentials is preferred here, because it

allows a more straightforward treatment of the integral equations arising in the microstrip surface-current determination.

The potentials are expressed as Sommerfeld integrals in the complex plane of the radial component k_ρ of the wave vector. The following shorthand notation will be used here for these integrals:

$$S_n[f] = \int_C H_n^{(2)}(k_\rho \rho) k_\rho^{n+1} f(k_\rho)\, dk_\rho \tag{3}$$

where $H_n^{(2)}$ is the Hankel function of nth order and ρ is the source/observer distance.

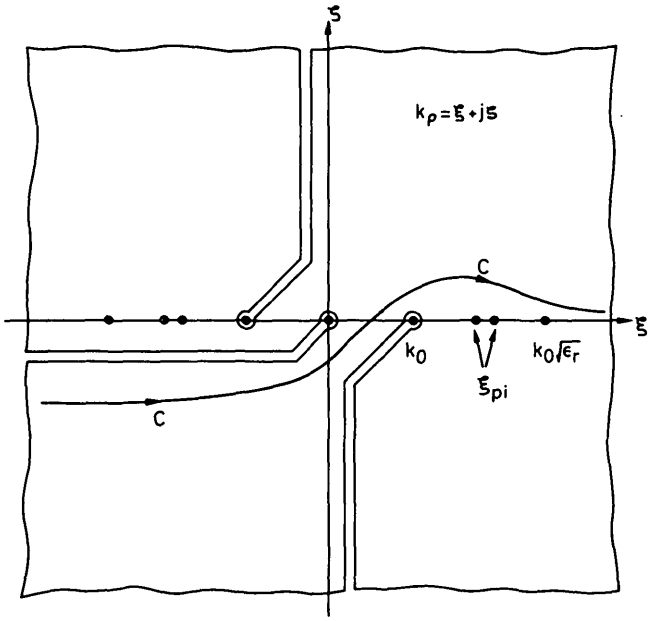

Fig. 2 *The complex plane k_ρ, showing the integration path C for the Sommerfeld integrals and a possible choice for the pertinent branch cuts*

C is an infinite path going through the third and first quadrant in the complex plane $k_\rho = \xi + j\,\zeta$, (Fig. 2). As a matter of fact, if the path C can be deformed into the real axis, $S_n[f]$ is the Hankel transform of the function $2k_\rho^n f$.

The following results are obtained for the potentials, by application of general stratified media theory [10]:

$$A_x = \frac{\mu_0}{4\pi} S_0 \begin{Bmatrix} \exp(-u_0 z)/D_{TE} \\ \sinh u(z+h)/(D_{TE} \sinh uh) \end{Bmatrix} \tag{4}$$

$$A_z = -\frac{\mu_0}{4\pi}(\epsilon_r - 1)\cos\phi S_1 \begin{Bmatrix} \exp(-u_0 z)/(D_{TE}D_{TM}) \\ \cosh u(z+h)/(D_{TE}D_{TM}\cosh uh) \end{Bmatrix} \tag{5}$$

$$V = \frac{\cos\phi}{4\pi j\omega\epsilon_0} S_1 \begin{Bmatrix} \exp(-u_0 z)N/(D_{TE}D_{TM}) \\ \sinh u(z+h)N/(D_{TE}D_{TM}\sinh uh) \end{Bmatrix} \tag{6}$$

where the upper and lower functions inside the symbol { } correspond, respectively, to air ($z > 0$) and the dielectric substrate ($-h < z < 0$).

In the above expressions the terms u_0 and u are related to the z-components of the wave vector in air and dielectric, respectively, by

$$u_0 = jk_{z0} = (k_\rho^2 - k_0^2)^{1/2} \tag{7}$$

$$u = jk_z = (k_\rho^2 - \epsilon_r k_0^2)^{1/2} \tag{8}$$

with $k_0^2 = \omega^2 \mu_0 \epsilon_0$.

The terms D_{TE}, D_{TM} and N, arising in the integrands, are given by

$$D_{TE} = u_0 + u\coth uh \tag{9}$$

$$D_{TM} = \epsilon_r u_0 + u\tanh uh \tag{10}$$

$$N = u_0 + u\tanh uh \tag{11}$$

where h is the substrate height.

In particular, D_{TE} and D_{TM} are closely linked to the Fresnel reflection coefficients R_{TE} and R_{TM} of a TE- or TM-wave, respectively, illuminating a dielectric-coated conductor [6] by the simple relations:

$$R_{TE} = 2u_0/D_{TE} - 1 \tag{12}$$

$$R_{TM} = 1 - 2u\tanh uh/D_{TM} \tag{13}$$

Thus, the zeros of D_{TE} and D_{TM} give the phase constant of the characteristic TE- and TM-modes propagating in such a structure [9]. For a lossless substrate they are situated on the segments $[|k_0|, |k_0\sqrt{\epsilon_r}|]$ of the real axis $\xi = \mathrm{Re}(k_\rho)$ (Fig. 2). As these zeros correspond to poles of the integrands, care must be taken when deforming the integration path into the real axis. After using the symmetry properties of $H_n^{(2)}$, the following general relationship holds:

$$S_n[f] = 2PV\int_0^\infty J_n(\xi\rho) f(\xi)\xi^{n+1}\, d\xi - 2\pi j\sum_i R_i\, \xi_{pi}^{n+1}\, J_n(\xi_{pi}\rho) \tag{14}$$

where R_i is the residue of f at the pole ξ_{pi}, and the integral is to be considered as a Cauchy principal value.

For the sake of completeness, the expressions for the tangential fields derived from eqns. 5–6 are given below for points on the interface:

$$4\pi j\omega\epsilon_0 E_\rho/\cos\phi = S_0[(k_0^2 D_{TM} + k_\rho^2 N)/(D_{TE}D_{TM})] + S_1[N/(D_{TE}D_{TM})]/\rho \tag{15}$$

$$4\pi j\omega\epsilon_0 E_\phi/\sin\phi = -S_0[k_0^2/D_{TE}] + S_1[N/(D_{TE}D_{TM})]/\rho \tag{16}$$

$$4\pi H_\rho/\sin\phi = -S_0[u_0/D_{TE}] + (\epsilon_r - 1)S_1[1/(D_{TE}D_{TM})]/\rho \tag{17}$$

$$4\pi H_\phi/\cos\phi = S_0[(\epsilon_r - 1)k_\rho^2 - u_0 D_{TM}/(D_{TE}D_{TM})] - (\epsilon_r - 1)S_1[1/(D_{TE}D_{TM})]/\rho \tag{18}$$

The normal components can also be derived from eqns. 4–6. In particular, it can be easily verified that the E_z component exhibits the expected discontinuity when crossing the air/dielectric interface.

3 Arbitrary upper conductor

For a general microstrip structure, with an arbitrary shaped upper conductor S supporting an electric current surface density J_s (Fig. 3), the fields can still be derived from eqns. 1 and 2. But now the potentials are expressed in terms of Green's functions as

$$A(r) = \int_s \bar{\bar{G}}_A(r|\rho')\cdot J_s(\rho')\, ds' \tag{19}$$

$$V(r) = \int_s G_v(r|\rho')\rho_s(\rho')\, ds' \tag{20}$$

These expressions are the starting point to establish an integ-

ral equation giving the currents and charges in any microstrip structure with a known excitation. Nevertheless, the solution of such an equation will not be attempted in this paper, which is mainly concerned with study of the associated Green's functions.

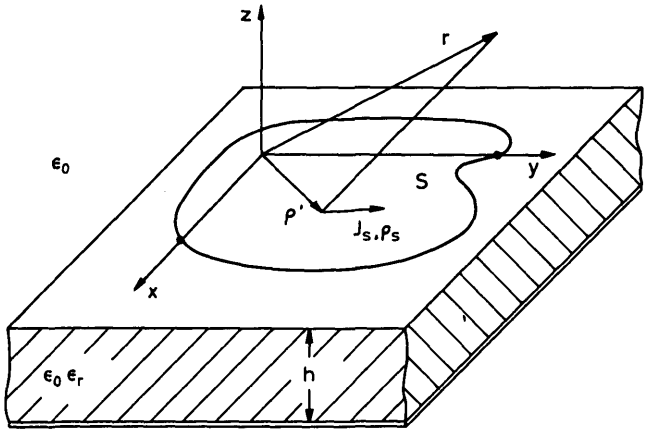

Fig. 3 *Microstrip structure with arbitrarily shaped upper conductor*

Here $\bar{\bar{G}}_A$ is a dyadic Green's function whose scalar component G_A^{st} is defined as the s-component of the vector potential created by an HED directed along the t-co-ordinate. Therefore, the xy- and yx-components are null elements in the dyadic, whereas the xx- and zx-components are to be identified with terms A_x and A_z given by eqns. 4 and 5. G_A^{yy} and G_A^{zy} may also be derived from eqns. 4 and 5 by symmetry considerations. Finally, the three components G_A^{sz} are irrelevant because no surface current is allowed in the z-direction.

The surface charge density associated with the scalar potential is $\rho_s = -\nabla . J_s/j\omega$, and the corresponding Green's function G_V is defined as the scalar potential of a single point charge, which is given by

$$G_V(r|\rho' = 0) = \frac{1}{4\pi j\omega\epsilon_0} S_0 \left\{ \begin{array}{l} \exp(-u_0 z)N/(D_{TE}D_{TM}) \\ \sinh u(z+h)N/ \\ (D_{TE}D_{TM} \sinh uh) \end{array} \right\} \tag{21}$$

This potential must not be mistaken with the scalar potential of an HED given by eqn. 6 which is, in fact, related to the tangential derivative of G_V.

4 Near- and far-field approximations

The integrals for the fields and the potentials have no analytical solution. However, it is possible to perform approximately the integration in the particular cases of the near and far fields. These situations are characterised by the mathematical conditions $k_0 \rho \ll 1$ and $k_0 \rho \gg 1$, and they will be illustrated here for the Green's functions G_V and G_A^{xx}, from which the tangential electric field of an arbitrary microstrip structure can be derived.

Near-field approximations are obtained by noting that the term u can be written as

$$u^2 = u_0^2 - (\epsilon_r - 1)k_0^2 \tag{22}$$

Thus, the obvious simplification is to make $u = u_0$ in the Sommerfeld integrals. With this substitution, analytical integration is possible and the following approximate expressions, valid in air, are obtained:

$$G_A^{xx}(k_0\rho \ll 1) = \frac{\mu_0}{4\pi}\left[\frac{\exp(-jk_0 r_0)}{r_0} - \frac{\exp(-jk_0 r_1)}{r_1}\right] \tag{23}$$

$$G_V(k_0\rho \ll 1) = \frac{1-\eta}{4\pi j\omega\epsilon_0}\left[\frac{\exp(-jk_0 r_0)}{r_0} - (1+\eta)\sum_{i=1}^{\infty}(-\eta)^{i-1}\frac{\exp(-jk_0 r_i)}{r_i}\right] \tag{24}$$

with

$$r_i^2 = \rho^2 + (z+2ih)^2 \tag{25a}$$

and

$$\eta = (\epsilon_r - 1)/(\epsilon_r + 1) \tag{25b}$$

It can be seen from the above expressions that, in the near field, the vector potential is unaffected by the permittivity of the substrate. On the other hand, the near-field approximation for the scalar potential can be viewed as an extension of the static Silvester's potential in microstrip [11], whose expression is obtained by making $k_0 = 0$ in eqns. 21 or 24.

The scalar potential of an HED is found by differentiating eqn. 24 with respect to x, and fields are derived in the usual way. For instance, the near-field approximation for the tangential electric field of an HED is:

$$E_t = -e_x \frac{j\omega\mu_0}{4\pi}\left[\frac{\exp(-ik_0 r_0)}{r_0} - \frac{\exp(-jk_0 r_1)}{r_1}\right] - \frac{1-\eta}{4\pi j\omega\epsilon_0}\nabla_t \times \left[\cos\phi\left[\frac{(1+jk_0 r_0)\rho}{r_0^3}\exp(-jk_0 r) - (1-\eta)\sum_{i=1}^{\infty}(-\eta)^{i-1}\frac{(1+jk_0 r_i)\rho}{r_i^3}\times \exp(-jk_0 r_i)\right]\right] \tag{26}$$

A similar expression has been derived by Chow and El-Behery [12] on a purely intuitive physical basis. The more crude approximation recently published by Hansen [13] is included in eqn. 26 as a particular case, obtained at zero frequency, if the contribution from the vector potential is neglected and only one term is taken in the infinite series for the scalar potential.

Far-field approximations can be obtained with standard asymptotical techniques, such as the steepest descent method [5, 7]. The main contributions to the asymptotic expansion arise here from the saddle point and from the poles on the real axis ξ. They correspond, respectively, to the spatial wave (geometrical optics field) and to the surface wave terms.

When both source and observer are in the air/dielectric interface the saddle point contribution vanishes and the fields show the typical behaviour of a surface wave, decreasing as the inverse square root of the distance ρ. As the dominant TM-mode in a grounded dielectric slab has zero cutoff frequency, the term D_{TM} always has at least one zero and the scalar potential always includes a surface-wave term. In opposition, the term D_{TE} has no zeros if the operating frequency satisfies the condition

$$f < \frac{c_0}{4h(\epsilon_r - 1)^{1/2}} \tag{27}$$

Thus we must resort to the following asymptotical term which comes from the branch point $\xi = k_0$ and is of the order $1/\rho^2$.

Under the condition given by eqn. 27, the leading terms in the asymptotical expansions of the Green's functions under consideration are, for $z = 0$:

$$G_A^{xx}(k_0\rho \gg 1) = \frac{\mu_0}{4\pi} \frac{\tan^2\Delta}{\Delta^2} \frac{2j\exp(-jk_0\rho)}{k_0\rho^2}$$

$$= \left(\frac{\tan\Delta}{\Delta}\right)^2 G_A^{xx}\ (\epsilon_r = 1) \tag{28}$$

$$G_V(k_0\rho \gg 1) = -2\pi j R_1 \xi_{p1}^2 H_0^{(2)}(\xi_{p1}\rho) \tag{29}$$

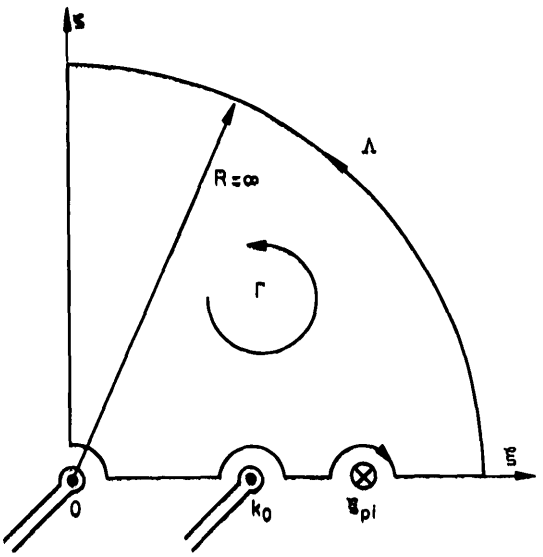

Fig. 4 *Closed path* Γ *in the complex plane* k_ρ

where $\Delta = k_0 h\sqrt{\epsilon_r - 1}$ and R_1 is the residue of $N/D_{TE}D_{TM}$ at the pole ξ_{p1}.

A point worth mentioning in eqn. 28 is that the ratio between asymptotical expansions for the inhomogeneous and homogeneous ($\epsilon_r = 1$) vector potentials is a real positive constant. On the other hand, eqn. 29 cannot be applied to the homogeneous case because the pole and branch point coincide. In fact, the pole contribution can hardly be separated from the nearby branch-point contribution in many practical situations, and a uniform asymptotic expansion [5] is needed for more accurate results.

5 Alternative formulation of Sommerfeld integrals

Sommerfeld integrals can be numerically evaluated by using eqn. 14, where they are expressed as a principal-value integral of a function oscillating over the real positive axis ξ. Prior to the development of a numerical technique to evaluate such integrals, an alternative formulation which avoids the singularity and offers several numerical advantages will be discussed here.

Let us consider the related complex integral:

$$I = \oint_\Gamma H_n^{(1)}(k_\rho\rho)\, k\rho^{n+1} f(k_\rho)\, dk_\rho = 0 \tag{30}$$

which vanishes because of the analyticity of the integrand inside the closed path Γ (Fig. 4).

The residues at the branch points $k_\rho = 0$ and $k_\rho = k_0$ are zero and, taking into account the asymptotic behaviour of the Hankel function, the contribution from the circular segment Λ also vanishes. On the imaginary axis the Hankel function of imaginary argument is transformed in a modified Bessel function K_n. Finally, eqn. 30 is expanded as

$$PV\int_0^\infty H_n^{(1)}(\xi\rho)\,\xi^{n+1} f(\xi)\, d\xi - \pi j \sum_i R_i \xi_{pi}^{n+1} H_n^{(1)}(\xi_{pi}\rho)$$

$$-\frac{2}{\pi}\int_0^\infty K_n(\zeta\rho)\,\zeta^{n+1} j f(j\zeta) d\zeta = 0 \tag{31}$$

On the segment $\xi > k_0$ of the real axis the function f is always real. Thus, taking the real part of eqn. 31, and making use of eqn. 14, the following alternative expression of Sommerfeld integrals is obtained:

$$S_n[f] = \frac{4}{\pi}\int_0^\infty K_n(\zeta\rho)\,\zeta^{n+1}\,\mathrm{Re}\,[jf(j\zeta)]\, d\zeta$$

$$+ 2j\int_0^{k_0} H_n^{(2)}(\xi\rho)\,\xi^{n+1}\,\mathrm{Im}\,[f(\xi)]\, d\xi$$

$$-2\pi j\sum_i R_i \xi_{pi}^{n+1} H_n^{(2)}(\xi_{pi}\rho)$$

$$= T_1 + T_2 + T_3 \tag{32}$$

and, now, no singularities arise in the functions to be integrated.

Eqn. 32 is also very interesting from a theoretical point of view, because it shows that Sommerfeld integrals can always be decomposed into three terms:

(*a*) A purely real term, corresponding to the integral over the imaginary axis. It must be considered as a static term giving the dominant contribution in the near field and becoming negligible in the far field.

(*b*) An integral over the $[0, k_0]$ interval (visible spectrum) of elementary waves propagating in the ρ- and z-directions. This is the spatial radiated wave which gives the dominant term in the far field except for points close to the interface.

(*c*) The surface wave propagating along ρ and decreasing exponentially along z. This gives the dominant contribution to the integral in the far field for points at the interface.

In fact, using k_z as the new dummy variable in the integrals of eqn. 32 leads to the classical radial transmission representation [5], in contrast with the z-transmission representation of Sommerfeld integrals given by the eqn. 14.

6 Numerical techniques

The radial transmission representation (eqn. 32) is particularly suited for numerical evaluation if $k_0\rho \gg 1$. Then, the asymptotic behaviour of the function to be integrated over $[0, \infty]$ is dominated by the strong exponential decrease of $K_n(\zeta\rho)$, and specially tailored techniques such as the Squire's algorithm [14] give a fast and accurate evaluation. The second integral in eqn. 32 has an oscillating integrand, but over a finite interval.

An extension of Filon's classical algorithm [15], in which the function Im (f) is approximated by parabolic interpolation and the integration performed analytically, has been found very useful.

Unfortunately, these algorithms lose their accuracy for small values of ρ and we must come back to the z-transmission representation (eqn. 14). Sommerfeld integrals, as given by eqn. 14, can be included in a more general kind of integral defined by

$$I(\rho) = \int_a^\infty g(\xi\rho) f(\xi)\, d\xi \tag{33}$$

where

(a) $g(\xi\rho)$ is a real oscillating function with a strictly periodic behaviour (sin, cos), or behaving asymptotically as the product of a periodic function and a monotonic function. A typical example of this class of functions, which will be termed from now on as quasiperiodical, are the Bessel functions of first kind.

(b) $f(\xi)$ is a complex function which behaves asymptotically as $O(\xi^\alpha)$. Therefore, for $\alpha > 0$, the integrand may diverge and the integral I must be considered in the Abel or mean sense. In addition, $f(\xi)$ can exhibit a finite number of isolated discontinuities for real values of ξ.

(c) The integration interval can be extended in the limiting case to the whole real axis ($a = -\infty$). In these situations, the infinite interval must be split into two semi-infinite intervals, prior to the application of subsequent developments.

As a typical example, Fig. 5 depicts the complex integrand

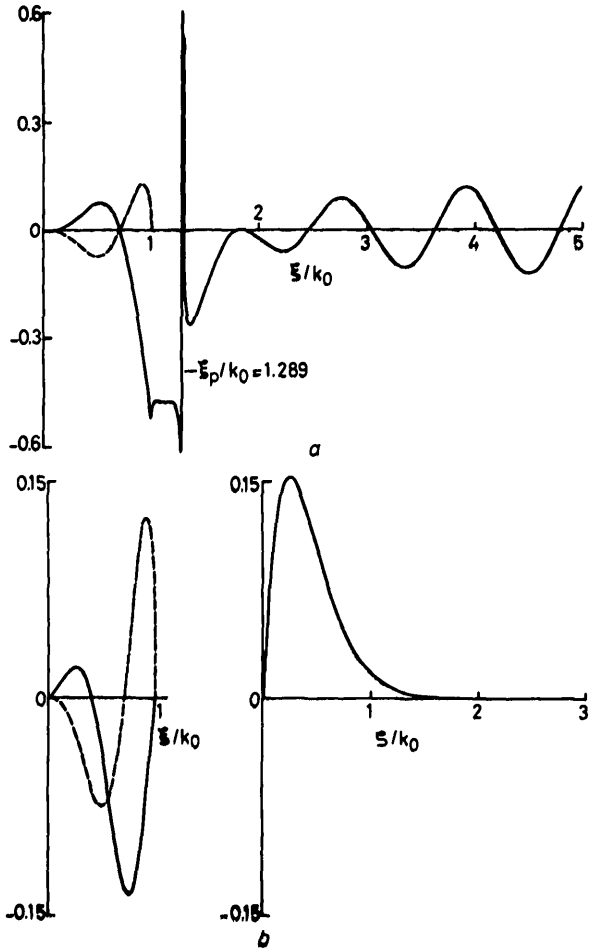

Fig. 5 *The functions to be integrated for the evaluation of the scalar potential V*
$z = 0; k_0\rho = 5.4; k_0 h = 0.2\pi; \epsilon_r = 5$

——— real part
– – – – imaginary part
a z-transmission formulation
b radial transmission formulation

of the Green's function G_V when $z = 0, k_0\rho = 5.4, \epsilon_r = 5$ and $k_0 h = 0.2\pi$. It can be seen that, in addition to the pole at $\xi/k_0 = 1.289$, a discontinuity in the derivative arises in the branch point at $\xi/k_0 = 1.0$. The integration of such a function by a crude numerical quadrature, using standard Gaussian or Newton-Cotes rules, is a very inefficient process calling for a very high number of integration points to achieve reasonable accuracy. In practical situations, like solving integral equations by moment methods, these integrals must be calculated a very large number of times so that even a slight reduction of the number of integration points, for a fixed accuracy, can improve the overall computation time considerably.

Sommerfeld integrals have been extensively investigated, from a numerical point of view, for the problem of radio-wave propagation above a lossy ground, where the comprehensive monograph of Lytle and Lager is the classical reference [16]. These authors have found an iterative Romberg integration satisfactory, as here the integrand displays an exponential convergence and its poles have been removed from the real axis. In microstrip problems, Romberg integration has also been used [8], but its effectiveness decreases considerably in the absence of a well behaved integrand.

In recent years, there has been a considerable amount of work published on the numerical evaluation of Fourier transforms, which are included in eqn. 33 as a particular case. The techniques involved can be classified in three groups.

(a) The decomposition $[a, \infty] = [a, A] + [A, \infty]$ Here, Filon's algorithm is applied to the finite interval $[a, A]$, while an asymptotical expression of the integrand is used to estimate the integral's value over $[A, \infty]$ approximatively [17]. The most serious drawbacks of this approach are the choice of A and the analytical work required; features which are hardly included in an automatic computation routine.

(b) Another approach applies if $g(\xi\rho)$ is a strictly periodical function; then the following decomposition is used:

$$\int_a^\infty g(\xi\rho) f(\xi)\, d\xi = \int_a^{a+p} g(\xi\rho) \sum_{n=0}^{\infty} f(\xi + np)\, d\xi \tag{34}$$

where p is the period of the function g. The infinite sum inside the integration sign can be evaluated by standard devices, such as Euler's transformation. Recently, a more involved technique using theoretical Fourier-transform concepts has been described in connection with a problem on quantum-mechanics impact cross-sections [18]. These methods work very well for high values of ρ and an exponentially decreasing integrand. Unfortunately, their extension to quasiperiodical diverging integrands seems problematic.

(c) The third group of techniques, introduced by Hurwitz and Zweifel [19], are defined by the decomposition

$$\int_a^\infty g(\xi\rho) f(\xi)\, d\xi = \sum_{n=0}^{\infty} \int_{a+np/2}^{a+(n+1)p/2} g(\xi\rho) f(\xi)\, d\xi \tag{35}$$

The integration over each half cycle is performed prior to the series' summation. As before, an accelerating device, such as Shanks' nonlinear transformation, can also be used to sum the infinite series [20].

This last technique, also known as the method of averages, is considered the most promising for application to Sommerfeld integrals and will be developed in the following Section.

7 The method of averages

The method of averages will be illustrated here for the particular choice $g(\xi\rho) = \cos \xi\rho$. Extension to other oscillating functions is straightforward. The series in eqn. 35 is evaluated

by considering the partial sums

$$I_m^1 = \int_a^{\xi_m} \cos \xi\rho\, f(\xi)\, d\xi \tag{36}$$

where $\xi_m = a + m\pi/\rho$. The error of I_m^1 can be estimated by integrating by parts over the interval $[\xi_m, \infty]$, with the result

$$I - I_m^1 \simeq -\frac{1}{\rho} f(\xi_m) \sin \xi_m \rho \tag{37}$$

This shows that the sequence I_m^1 oscillates around the true value I, the best results being obtained if the ξ_m values are chosen as the extrema of the function g.

A new sequence I_m^2 is found by taking the average of two consecutive values in the sequence I_m^1, following the general expression

$$I_m^{n+1} = (I_m^n + I_{m+1}^n)/2 \tag{38}$$

and now the application of eqn. 37 in eqn. 38 gives

$$I - I_m^2 \simeq \frac{\pi}{2\rho^2} f'(\xi_m) \sin \xi_m \rho \tag{39}$$

so the sequence I_m^2 also has an oscillatory behaviour around I. Subsequent use of eqn. 38 produces new sequences I_m^n. Taking into account the asymptotic behaviour $f(\xi) = O(\xi^{\alpha})$, the sequences with $n > \alpha + 1$ converge towards the true value I. The last sequence reduces to a single value explicitly given by

$$I_1^M = 2^{1-M} \sum_{m=1}^{M} \binom{M-1}{m-1} I_m^1 \tag{40}$$

Hence, I_1^M will be closer to I than any value I_m^1; in spite of the fact that no new evaluations of the integrand have been required.

The convergence of this algorithm can be accelerated if the arithmetical mean of eqn. 38 is replaced by a weighted mean

$$I_m^{n+1} = (w_m^n I_m^n + w_{m+1}^n I_{m+1}^n)/(w_m^n + w_{m+1}^n) \tag{41}$$

in which the weights increase with m. Their optimum value, obtained upon consideration of eqns. 37 and 40, is

$$w_m^n = (\xi_1/\xi_m)^{\alpha+1-n} \tag{42}$$

with this choice, the method of averages is a very efficient technique, which may also be used with the Bessel functions J_n, replacing $f(\xi)$ by $(2/\pi\xi\rho)^{1/2} f(\xi)$ and $g(\xi\rho)$ by $\cos(\xi\rho - \pi/4 - n\pi/2)$. When applying the method of averages to the integrals of eqns. 4–6 and eqns. 15–18, an additional difficulty arises if some poles are present in the integrand, the integral being then defined as a principal value. In this case, a special integration technique, such as the 'folding around the pole technique' [10], must be used in the half cycle containing the singularity.

8 Results

To establish a numerical comparison between the formulations of eqns. 14 and 32, the Sommerfeld integrals $S_0[k_\rho/u_0]$ and $S_0[k_\rho/\{u_0(1 + \coth u_0 h)\}]$, which correspond to the vector potential of a HED in the free space and the homogenous microstrip, respectively, have been calculated.

Extensive tests performed in the range $0.001 < k_0\rho < 100$ and $0.01 < k_0 h < 1.5$ show that usually the z-transmission formulation (eqn. 14) is numerically more adequate for values $k_0\rho < 2\pi$, i.e. for distances less than one wavelength in free space.

Unfortunately, numerical tests are not possible when a pole exists on the real axis, because no analytical solution is known in these cases. As an alternative to Fig. 5*a*, Fig. 5*b* shows the function to be integrated if the radial transmission formulation is used instead of the z-formulation. Some tests performed on related principal value integrals indicate that one wavelength in free space is still a good dividing point between the two formulations.

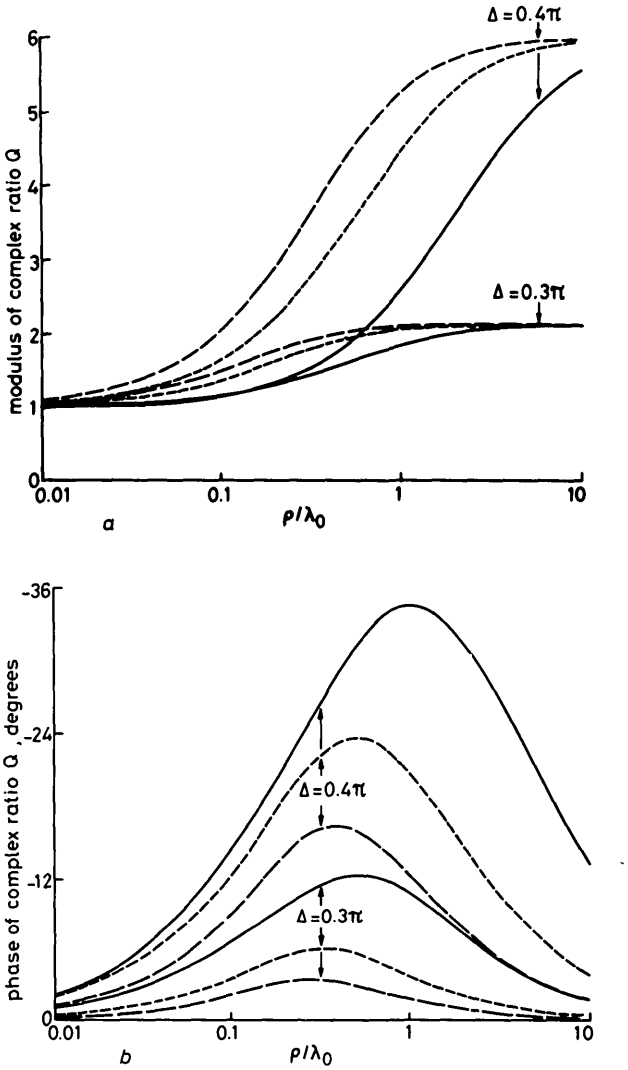

Fig. 6 *Complex ratio Q as a function of the normalised distance for z = 0, and several values of permittivity and normalised substrate thickness*

——— $\epsilon_r = 2$
– – – – $\epsilon_r = 5$
— — — $\epsilon_r = 10$
a Modulus, *b* phase

With these facts in mind, the x-component of the vector potential, as given by eqn. 4, has been calculated in the air/dielectric interface. Because A_x is closely related to its homogeneous counterpart in the near and far fields, it is more instructive to consider the complex ratio $Q = A_x/A_x$ ($\epsilon_r = 1$). The computer generated plots of Figs. 6*a* and *b* show the modulus and argument of Q, respectively, against the radial distance measured in free-space wavelengths. The cases $\epsilon_r = 2$, 5, 10 and $\Delta = 0.3\pi$, 0.4π have been depicted. The numerical results validate the near- (eqn. 23) and far- (eqn. 28) field approximations: the modulus of Q ranges between 1 and $(\tan\Delta/\Delta)^2$ while the argument reaches a maximum; whose value depends on ϵ_r and h, and vanishes in the near and far fields.

The situation is very different for the scalar potential of a point charge, which defines the Green's function G_V. In

Figs. 7*a* and *b* the modulus and phase of the normalised potential $G_{VN} = 4\pi j(\epsilon_0/\mu_0)^{1/2} G_V$ have been plotted against the normalised radial distance for $\epsilon_r = 5$, and normalised substrate thickness $h/\lambda_0 = 0.025$, 0.050 and 0.100. For instance, with $h = 1.5$ mm, these values correspond to the frequencies 5, 10 and 20 GHz. The near- and far-field approximations, eqns. 24 and 29, are represented by discontinuous lines.

It can be seen that the near-field approximation gives only reasonable results for $\rho/\lambda_0 < 0.1$ and small values of h/λ_0. In opposition, the surface-wave behaviour is reached more rapidly for electrically thicker substrates. Also, there is a transition zone between the quasistatic (ρ^{-1}) and surface-wave ($\rho^{-1/2}$) dependence, which becomes more marked for small values of h/λ_0. This transition zone appears as a rapid variation of the phase (Fig. 7*b*), which rises sharply from small positive values and afterwards follows a typical surface-wave pattern. In Fig. 7*b* the phases of the near- and far-field approximations have been plotted only in the case $h/\lambda_0 = 0.100$.

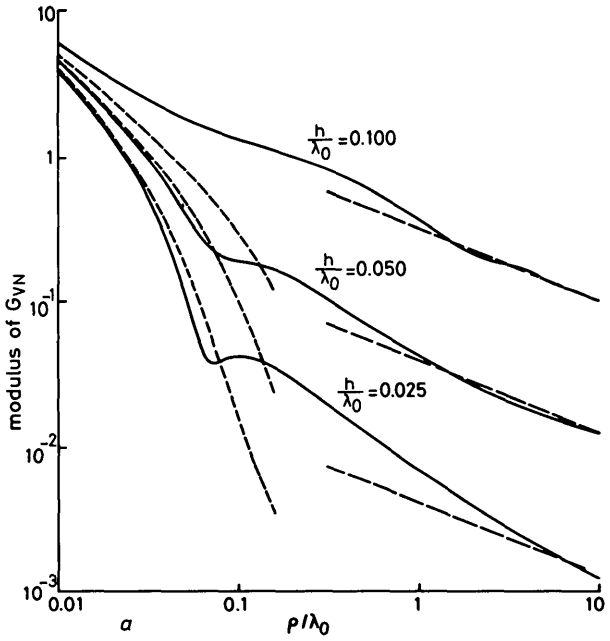

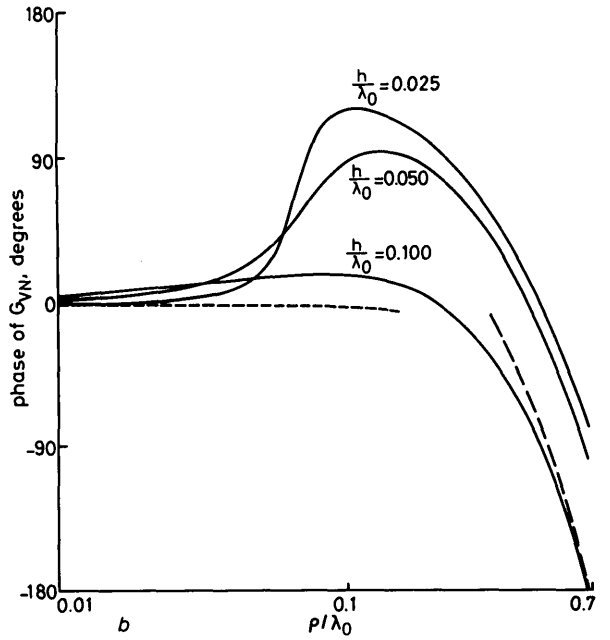

Fig. 7 *Normalised Green's function G_{VN}, for $z = 0$, $\epsilon_r = 5$ and various normalised substrate thicknesses*

------ near-field approximation ($h/\lambda_0 = 0.1$)
——— far-field approximation ($h/\lambda_0 = 0.1$)
a Modulus, *b* phase

More insight into these phenomena can be obtained by keeping h/λ_0 to a constant value, and changing ϵ_r. The cases $h/\lambda_0 = 0.01$ and $\epsilon_r = 1$, 2, 5 and 10 have been presented in Fig. 8. The curves for $\epsilon_r \neq 1$ follow closely the homogeneous behaviour, except for a scaling factor $(\epsilon_r + 1)/2$, until a transition zone, after which the surface wave becomes dominant. A point worth mentioning is that for $\epsilon_r = 10, h = 0.64$ mm and, consequently, a frequency of 4.69 GHz, the near-field approximation cannot be extended beyond $\rho/\lambda_0 = 0.03$; the distance corresponding to a relative minimum in the modulus of the potential.

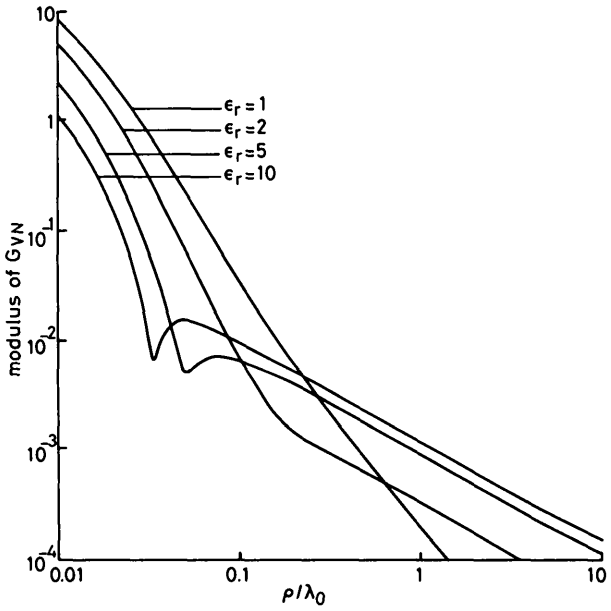

Fig. 8 *Modulus of the normalised Green's function G_{VN}, for $z = 0$, $h/\lambda_0 = 0.01$ and various permittivities*

As a final exemple, the radial transmission decomposition (eqn. 32) has been investigated for the integral associated with the scalar potential V of an HED, eqn. 6. Actually, this integral also gives the radial electric field of a point charge on microstrip. The normalised modulus of the integral $V_N = 4\pi j V/\omega\mu_0 \cos\phi$, for $\epsilon_r = 10$ and $h/\lambda_0 = 0.02$, is plotted as a continuous line in the Fig. 9, while the three terms T_i are represented by discontinuous lines. The real term T_1 is the dominant term in the near field, until the sharp minimum denoting the beginning of the transition zone. After this zone, the term T_2 gives the main contribution to the potential, but it is rapidly overtaken by the surface wave (T_3). The near-field approximation has also been included as a dotted line. This approximation is essentially different from the T_1 term, which, in fact, vanishes in the transition zone to take after small negative values.

9 Conclusions

An exact theory has been developed for the calculation of the electromagnetic fields and the potentials created by an arbitrary surface-current distribution on microstrip. Special attention has been paid to the cases where both the source and the observer are situated in the air/dielectric interface.

The simplest cases, in which the source is a point charge or a horizontal electric dipole, have been studied extensively. The fields and the potentials are thus given by Sommerfeld integrals, for which two different formulations have been developed. Their theoretical meaning, as well as their adequacy to a numerical evaluation, have been discussed in detail.

The most salient feature of the results obtained for the potentials is their hybrid behaviour, which ranges between a quasistatic dependence in the near field and a surface-wave dependence in the far field; both regions being separated by a frequently abrupt transition zone. In fact, the quasistatic zone, and consequently the range of validity of any homogeneous approximation for the fields of a microstrip dipole, seems to go barely beyond $0.1\,\lambda_0$.

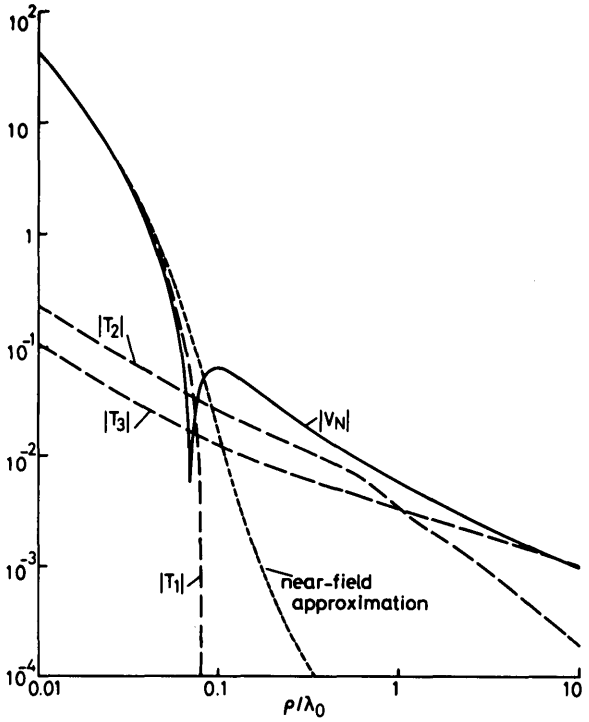

Fig. 9 *Normalised scalar potential V_N of a HED on microstrip and its radial-transmission decomposition*

$z = 0$, $\epsilon_r = 10$, $h/\lambda_0 = 0.02$
——— modulus of V_N
– – – – terms $|T_i|$
– – – – – near-field approximation

On the other hand, it is very difficult to predict the error which can be introduced in the resonant frequency, input impedance or radiation pattern of a microstrip antenna if such an approximation is used. Some preliminary results, obtained with the techniques developed in this paper, would tend to prove that quite accurate results may be expected for half wavelength or smaller antennas, whereas the behaviour of larger antennas or the coupling between distant elements of an array antenna cannot be correctly predicted if surface-wave effects are not included.

A definite quantitative answer to these questions can only be obtained if, in the standard EFIE-type integral equation, the free-space kernel is replaced by the exact kernel developed in this paper. Owing to the algorithms introduced here, this substitution can be performed with only a moderate increase of computational effort. Hence, the numerical techniques, currently used to solve the integral equations in free space, can be extended to microstrip problems, within reasonable limits for the overall computer time. Further work to quantitatively define the range of validity of the quasistatical approach is in progress, and the results will be reported in a later paper.

10 References

1 SANFORD, G.G.: 'Conformal microstrip phased array for aircraft tests with ATS-6', *IEEE Trans.*, 1978, **AP-26**, pp. 642–646
2 STERZER, F., PAGLIONE, R., NOWOGRODZSKY, M., and BECK, E.: 'Microwave apparatus for the treatment of cancer by hyperthermia', *Microwave J.*, 1980, **23**, pp. 39–44
3 RICHARDS, W.P., LO, Y.T., and HARRISON, D.D.: 'An improved theory for microstrip antennas and applications', *IEEE Trans.*, 1981, **AP-29**, pp. 38–46
4 WAIT, J.R.: 'Electromagnetic waves in stratified media' (Pergamon Press, 1970)
5 FELSEN, L.B., and MARCUVITZ, N.: 'Radiation and scattering of waves' (Prentice Hall, 1973)
6 KONG, J.A.: 'Theory of electromagnetic waves' (John Wiley and Sons, 1975)
7 UZUNOGLU, N.K., ALEXOPOULOS, N., and FIKIORIS, J.G.: 'Radiation properties of microstrip dipoles', *IEEE Trans.*, 1979, **AP-27**, pp. 853–858
8 MOSIG, J.R., and GARDIOL, F.E.: 'The near field of an open microstrip structure'. IEEE AP-S symposium, Seattle, USA, 1979, pp. 379–382
9 HARRINGTON, R.F.: 'Time-harmonic electromagnetic fields' (McGraw-Hill, 1961)
10 MOSIG, J.R.: 'A dynamic vector potential theory for three-dimensional microstrip structures', *Bull. AGEN*, 1978, pp. 45–52
11 SILVESTER, P., and BENEDEK, P.: 'Electrostatics of microstrip: revisited', *IEEE Trans.*, 1972, **MTT-20**, pp. 756–758
12 CHOW, Y.L., and EL-BEHERY, I.: 'An approximate dynamic spatial Green's function for microstrip lines', *ibid.*, 1978, **MTT-26**, pp. 978–983
13 HANSEN, V.: 'Approximate equations for the nearfield of a horizontal electric dipole on a grounded dielectric slab', *IEEE Proc. H, Microwaves, Opt. & Antennas*, 1982, **129**, (1), pp. 29–31
14 SQUIRE, W.: 'An efficient iterative method for numerical evaluation of integrals over a semi-infinite range', *Int. J. Number. Methods Eng.*, 1975, **9**, pp. 478–484
15 FILON, L.N.G.: 'On a quadrature formula for trigonometric integrals', *Proc. R. Soc. Edinburgh*, 1982, **49**, pp. 38–47
16 LYTLE, R.J., and LAGER, D.L.: 'Numerical evaluation of Sommerfield integrals'. Report UCRL-52423, Lawrence Livermore Laboratory, University of California, 1974
17 PANTIS, G.: 'The evaluation of integrals with oscillatory integrands', *J. Comput. Phys.*, 1975, **17**, pp. 229–233
18 BORIS, J.P., and ORAN, E.S.: 'Evaluation of oscillatory integrals', *ibid.*, 1975, **17**, pp. 425–433
19 HURWITZ, H., and ZWEIFEL, P.F.: 'Numerical quadrature of Fourier transform integrals', *Math. Tables Aids Comput.*, 1956, **10**, pp. 140–149
20 ALAYLIOGLU, A., EVANS, G.A., and HYSLOP, J.: 'The evaluation of oscillatory integrals with infinite limits', *J. Comput. Phys.*, 1973, **13**, pp. 433–438